

# Novel Two-Step Method for Synthesis of High-Density Nanocrystalline Diamond Fibers

Manoj K. Singh,\* E. Titus, J. C. Madaleno, G. Cabral, and J. Gracio

Centre for Mechanical Technology and Automation, Departamento de Engenharia Mecânica, Universidade de Aveiro, Campus de Santiago, 3810-193 Aveiro, Portugal

Received May 31, 2007. Revised Manuscript Received January 7, 2008

We report a novel two-step method for the fabrication of high-density nanocrystalline diamond (NCD) fibers with lengths of 50–100  $\mu\text{m}$  and diameters of 1–5  $\mu\text{m}$ . This method includes the synthesis of templates (silica ( $\alpha\text{-SiO}_2$ ) nanofibers) by a conventional vapor–liquid–solid method and the conformal coating of the nanofibers with 15–20 nm sized NCD grains by a microwave plasma enhanced chemical vapor deposition technique in hydrogen-deficient conditions. A detailed microstructural analysis was performed to probe the interaction of the NCD grains with  $\alpha\text{-SiO}_2$  nanofibers. The specimen for transmission electron microscopy (TEM) was prepared using the focused ion beam lift-out method. Elemental line profiles across the core–sheath region of the fiber were probed by energy-dispersive X-ray microanalysis in scanning TEM mode. Room temperature micro-Raman ( $\text{Ar}^+$  laser, 514 nm excitation wavelength, with a power of 25 mW) and parallel acquisition electron energy loss spectroscopy analysis were performed to study the crystalline quality of the NCD fiber. These novel materials may find applications in micro- and nanoelectromechanical systems and as heat sinks in microelectronics.

## Introduction

Diamond-coated metallic and nonmetallic wires are a new class of composite materials with excellent properties in terms of hardness, chemical inertness and thermal conductivity.<sup>1</sup> These composite structures have a better stiffness/weight ratio than any other existing material, and so have many potential applications in aerospace industry and water-jet cutting technology. The possibility of deposition of layered microdiamond coatings onto tungsten wires by the chemical vapor deposition method was demonstrated for the first time by May et al.<sup>2</sup> Later, many others reported the successful coating of microdiamond onto a variety of substrate wires including silicon carbide, copper, tungsten, and titanium.<sup>3–5</sup> Free-standing hollow diamond fibers were also formed from these diamond-coated wires by etching out the metal core. These tubes have potential applications in mechanical reinforcement and thermal management as well as in microelectronics. However, the difficulty in controlling the size, texture, and crystalline quality of the diamond grains and in achieving concrete coating is reflected in many of these works. There are many reports on growth of diamond films on  $\alpha\text{-SiO}_2$  surfaces using a high-power microwave plasma enhanced chemical vapor deposition (MPECVD)

technique;<sup>6–10</sup> however, no method of coating nanocrystalline diamond (NCD) onto silica ( $\alpha\text{-SiO}_2$ ) nanofibers has been reported.

In this work, we have demonstrated for the first time the facile fabrication and the conformal coating of NCD onto  $\alpha\text{-SiO}_2$  nanostructures by a two-step method: (i) synthesis of templates ( $\alpha\text{-SiO}_2$  nanofibers) on silicon wafer and (ii) coating of as-grown  $\alpha\text{-SiO}_2$  fibers with NCD diamond. A systematic study of the growth stages from nucleation to continuous fibrous structure formation (integration of NCD into nanofiber) has been performed. The interaction of diamond supergrains (collection of nanosized diamond grains) with  $\alpha\text{-SiO}_2$  nanofibers and their gradual transformation into nanodiamond fibers has been displayed. Nanodiamond-coated  $\alpha\text{-SiO}_2$  nanofibers can find potential applications in various strategic fields, such as biosensors,<sup>11,12</sup> energy saving, thermal management, and space technology.

## Experimental Section

The  $\alpha\text{-SiO}_2$  nanofibers were synthesized by conventional Vapor–Liquid–Solid (VLS) growth process.<sup>13–16</sup> A powder mixture of SiO (99.999%, Sigma Aldrich,  $\sim 100$  nm) and graphite (99.99%,

\* Corresponding author. E-mail: mksingh@ua.pt

- (1) May, P. W.; Portman, R.; Rosser, K. N. *Diamond Relat. Mater.* **2005**, *14*, 598.
- (2) May, P. W. *Endeavour* **1995**, *19*, 101.
- (3) Baranauskas, V.; Ceragioli, H. J.; Peterlevitz, A. C.; Durrant, A. F. *Thin Solid Films* **2001**, *398*, 250.
- (4) Chollon, G.; Naslain, R.; Prentice, C.; Shatwell, R.; May, P. J. *Eur. Ceram. Soc.* **2005**, *25*, 1929.
- (5) Lee, S. S.; Takai, O.; Itoh, H. *J. Mater. Sci.* **1997**, *32*, 2417.

- (6) Lee, J.; Liu, K.; Lin, I. *J. Appl. Phys.* **1997**, *81*, 486.
- (7) Irwina, M. D.; Pantano, C. G.; Gluche, P.; Kohn, E. *Appl. Phys. Lett.* **1997**, *81*, 716.
- (8) Sepulveda, N.; Aslam, D.; Sullivan, J. P. *Diamond Relat. Mater.* **2006**, *15*, 398.
- (9) Madaleno, J. C.; Singh, M. K.; Titus, E.; Cabral, G.; Grácio, J.; Pereira, L. *Appl. Phys. Lett.* **2007**, accepted.
- (10) Singh, M. K.; Titus, E.; Madaleno, J. C.; Pereira, L.; Cabral, G.; Neto, V. F.; Grácio, J. *Diamond Relat. Mater.* **2007**, accepted.
- (11) Xie, S.; Shafer, G.; Wilson, C. G.; Martin, H. B. *Diamond Relat. Mater.* **2006**, *15*, 225.
- (12) Martin, H. B.; Argoitia, A.; Angus, J. C.; Landau, U. *J. Electrochem. Soc.* **1999**, *146*, 2959.

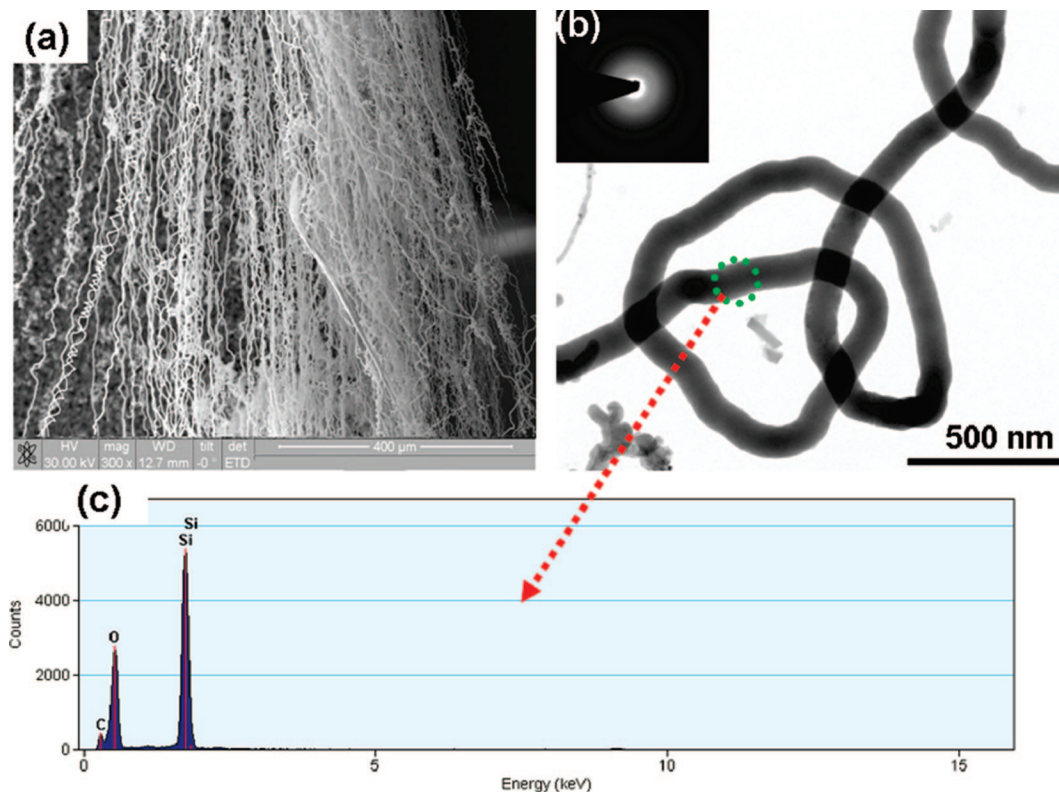


**Figure 1.** (a) FE-SEM image of high density  $a$ -SiO<sub>2</sub> nanofibers deposited randomly on a p type Si wafer by VLS technique. (b) Bright-field TEM image of  $\sim 100$  nm diameter  $a$ -SiO<sub>2</sub> nanofiber. Inset: diffuse rings in the SAED pattern that originate from  $a$ -SiO<sub>2</sub> nanofibers. (c) EDS spectrum taken from the nanofiber (exact location marked by a green-dotted circle in (b)), showing the presence of Si and O (1:2 ratio) in the sample; C comes from contamination during the preparation of TEM specimens.

Sigma Aldrich  $\sim 70$  nm) was kept in an alumina boat. An Au-catalyzed ( $\sim 100$  nm) Si substrate was placed closed to it, in the downstream side of flowing argon inside a hot furnace heated to 1000–1140 °C. The samples were taken out after being cooled to room temperature, and a white-colored deposit was observed on their surface.

Subsequently, the as-synthesized  $a$ -SiO<sub>2</sub> nanofiber templates were coated by NCD using a 2.45 GHz MPECVD system (ASTeX Corp.). Prior to NCD coating, substrates were treated by nanodiamond powder (grain size 3–5 nm) using the dip method.<sup>17</sup> By this treatment, nanodiamond particles were randomly attached on the surface of  $a$ -SiO<sub>2</sub> nanofibers by capillary forces. The nanodiamond particles acted as seeds for the further growth of NCD on  $a$ -SiO<sub>2</sub> nanofibers. The seeding process is a very critical phase for conformal coating as well as for controlling the diameter of NCD fibers.

The pretreated samples were placed inside a 2.45 GHz MPECVD system (ASTeX) and the NCD coating was performed for 15 min using 1% CH<sub>4</sub>, 89% Ar, and 10% H<sub>2</sub> at 120 Torr pressure. During the deposition, the substrate temperature was maintained at 700 °C and the microwave power was optimized for 800 W. The growth evolution of the NCD coating was investigated for samples deposited at two different deposition times, 5 and 15 min, respectively.

For the purpose of characterization, a field-emission scanning electron microscopy (FE-SEM, Hitachi S-800, 30 keV) was used to investigate the morphology of the produced nanostructures. Room temperature micro-Raman studies were performed with a Renishaw 1000 Raman spectroscope (Ar<sup>+</sup> laser beam spot diameter  $\sim 1$  μm, 514 nm excitation wavelength, with a power of 25 mW), to study the crystalline quality of the NCD fibers.

The specimen for transmission electron microscopy (TEM) of NCD fiber were prepared by using FEI Strata DB235 Focused Ion Beam (FIB) lift-out method.<sup>18</sup> FIB cutting was performed by accelerated gallium ions (Ga<sup>+</sup>) with an acceleration voltage of 30 keV and a beam current in the range 200–5000 pA. The high-resolution transmission electron microscopy (HR-TEM) measurements were carried out with 300 keV electrons using a FEI-Technai F30 microscope equipped with Gatan parallel electron energy loss spectrometer (PEELS). The spatial resolution was about 0.2 nm. Elemental line profiles across the core-sheath region of the fiber were probed by energy-dispersive X-ray microanalysis (EDS) in scanning TEM mode.

## Results and Discussion

Figure 1a shows the field-emission scanning electron microscopy image of as-grown  $a$ -SiO<sub>2</sub> nanofiber. High density nanofibers with lengths larger than 500 μm are apparent in the image. Figure 1b reveals the bright-field TEM image of nanofibers with diameter in the order of  $\sim 100$  nm. The corresponding EDS spectrum (Figure 1c) confirms the presence of Si and O (1:2 ratio) in the sample. The element

(13) Jeedigunta, S.; Singh, M. K.; Kumar, A. *J. Nanosci. Nanotechnol.* **2007**, *486*, 7.

(14) Jeedigunta, S.; Singh, M. K.; Kumar, A.; Zekri, S. *J. Nanosci. Nanotechnol.* **2006**, *640*, 6.

(15) Dai, Z. R.; Pan, Z. W.; Wang, Z. L. *Adv. Funct. Mater.* **2003**, *13*, 9.

(16) Lathon, L. J.; Gudixsen, M. S.; Wang, D.; Lieber, C. M. *Nature* **2002**, *420*, 57.

(17) Song, Y.; Kim, G. Y.; Choi, H. K.; Jeong, H. L.; Lee, Y. H. *Chem. Vap. Deposition* **2006**, *12*, 375.

(18) Mucha, H.; Kato, T.; Arai, S.; Saka, H.; Kuroda, K.; Weilage, B. *J. Electron Microsc.* **2005**, *54*, 43.



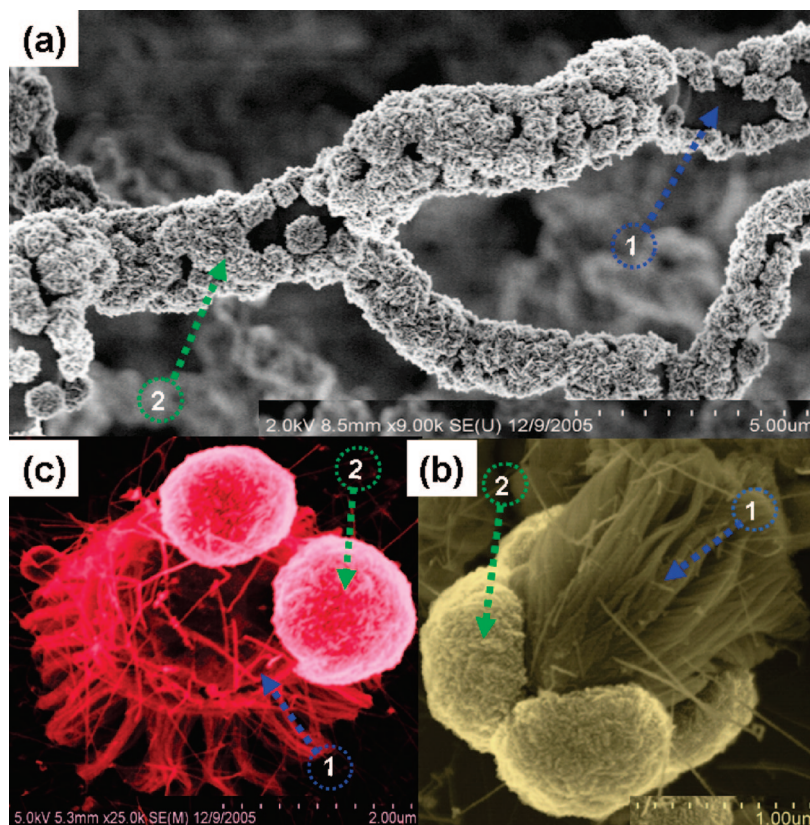


**Figure 2.** (a) FE-SEM image after 5 min NCD deposition, showing the interaction of diamond supergrains and *a*-SiO<sub>2</sub> nanofibers. (b, c) Highly magnified FE-SEM images, collected from various spots of the same sample. (1) Blue- and (2) red-dashed arrows point at the nanofiber surface and diamond supergrains, respectively.

C is the signature of the contamination from the carbon coated copper grids used during the preparation of TEM specimens by replica technique.<sup>19,20</sup> The amorphous structure of SiO<sub>2</sub> nanofibers was confirmed by Selected Area Electron Diffraction pattern (SAED) (inset of Figure 1b).

Using the FE-SEM, we have investigated the growth morphology of our product for two different time frames, 5 and 15 min, respectively. The information gathered from this analysis highlights a number of interesting features. First of all it, is evident that, under our experimental conditions, the process of NCD fiber synthesis is characterized by a very high growth rate. Figure 2a–c illustrates the FE-SEM image of the *a*-SiO<sub>2</sub> after 5 min NCD deposition. Amorphous SiO<sub>2</sub> nanofiber surface and the supergrains are indicated in Figure 2a–c by blue-dashed arrow 1 and red-dashed arrow 2, respectively. The supergrain shown in Figure 2a–c consists of many nanometer-sized crystalline diamond grains. Different supergrains can be observed on the nanofiber surface. These supergrains (200–500 nm in diameter) act as nucleation centers for further growth of diamond on *a*-SiO<sub>2</sub> nanofibers. The initial growth stage is evident and it is very prominent how diamond supergrain interacts with the *a*-SiO<sub>2</sub> nanofiber. A similar structure has been reported by Carlisle et al.<sup>21</sup> However, their hybrid structure was composed of ultrananocrystalline diamond (UNCD) and carbon nanotubes

(CNTs). The possible interaction of UNCD with the CNTs is not shown in any of their results. It is also very fascinating to see how a self-assembly of a bundle of *a*-SiO<sub>2</sub> nanofibers is integrated with diamond supergrains (see images b and c in Figure 2). From above images (Figure 2a–c), it seems that NCD supergrain loves to interact with *a*-SiO<sub>2</sub> nanofibers.

The low magnified FE-SEM image displaying the surface morphology of NCD-coated *a*-SiO<sub>2</sub> fiber achieved with 15 min CVD is exhibited in Figure 3a. Figure 3b shows a more magnified view of Figure 3a denoted by red dashed square. The random formation of NCD coated fibers ~100 μm in length is visible. High magnified FE-SEM image of the tip of branched NCD fiber is shown in Figure 3c (indicated by green-dotted circle with red dashed arrow). Figure 3d reveals isolated NCD fiber from the same sample with diameter ~3 μm, which reveals that *a*-SiO<sub>2</sub> nanofibers were conformally coated by nanodiamond with a very high growth rate.

Room temperature micro-Raman studies were performed to study the crystalline quality of the NCD fibers. An optical microscopic image (see Figure 4a) of the as-synthesized NCD fibers after 15 min CVD deposition locates the focusing of laser beam (spot diameter ~1 μm).

(19) Misra, A.; Singh, M. K.; Tyagi, P. K.; Misra, D. S.; Satyam, P. V. *Diamond Relat. Mater.* **2006**, *15*, 300.

(20) Tyagi, P. K.; Misra, A.; Singh, M. K.; Misra, D. S.; Satyam, P. V.; LeNorman, F. *Appl. Phys. Lett.* **2005**, *86*, 253110.

(21) Xiao, X.; Elam, J. W.; Trasobares, S.; Auciello, O.; Carlisle, J. A. *Adv. Mater.* **2005**, *17*, 1496.

(22) Sun, Z.; Shi, J. R.; Tay, B. K.; Lau, S. P. *Diamond Relat. Mater.* **2000**, *9*, 1979.

(23) Zhou, D.; Gruen, D. M.; Qin, L. C.; McCauley, T. G.; Krauss, A. R. *J. Appl. Phys.* **1998**, *84*, 1981.



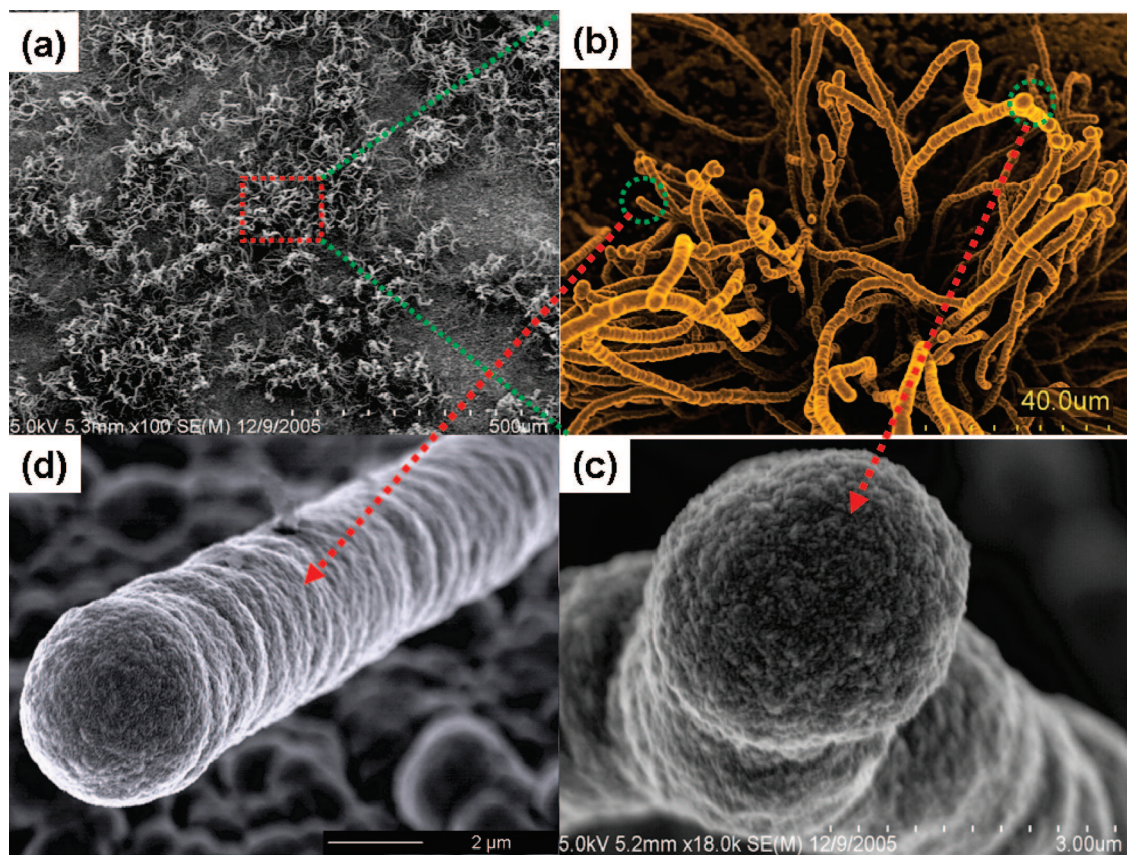


**Figure 3.** (a) FE-SEM image of NCD-coated fibers after 15 min of CVD. (b) Higher magnified view of the fibers. (c) High-magnification FE-SEM image of joint of two NCD fibers marked in (b). (d) Image of an isolated NCD fiber from the same sample with diameter  $\sim 3 \mu\text{m}$ , illustrating that  $\alpha\text{-SiO}_2$  nanofibers were conformally coated by nanodiamond with a very high growth rate.

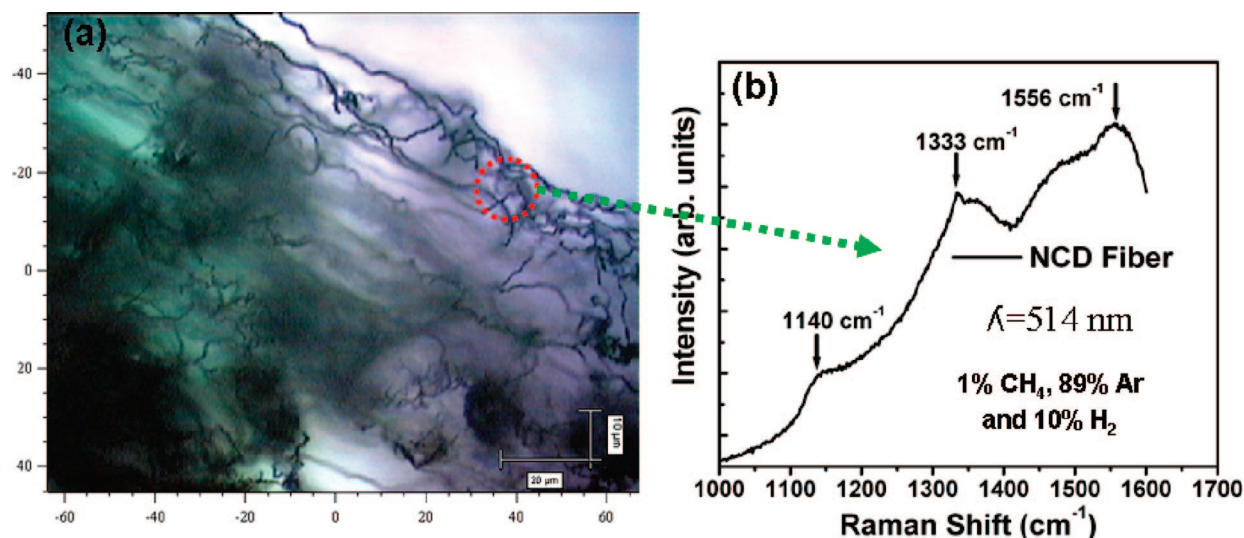


**Figure 4.** (a) Optical microscopic image of as-synthesized NCD fibers after 15 min of CVD. (b) Raman spectra of the NCD-coated fibers; bands at 1140, 1333, 1550, and 1460  $\text{cm}^{-1}$  are finger prints of NCD.<sup>22</sup>

The visible Raman spectra taken from the diamond fiber show several distinct features at 1140, 1333, 1460 and 1550  $\text{cm}^{-1}$  (see Figure 4b). The low intensity broad peak at  $\sim 1333 \text{ cm}^{-1}$  is attributed to the nanocrystalline diamond nature of fiber. The broadening of the Raman peak of diamond was also experimentally observed in small grain sized NCD powders by Sun et al.<sup>22</sup> and Zhou et al.<sup>23</sup>. It is widely believed that peaks at 1140 and 1460  $\text{cm}^{-1}$  originate from

the presence of confined phonon modes in diamond.<sup>24,25</sup> The peak at 1550  $\text{cm}^{-1}$  is clearly attributed to the G-mode Raman peak, which is well-known for disordered carbon films and arises from the in-plane stretching modes of the  $\text{sp}^2$ -bonded

(24) Nemanich, R. J.; Glass, J. T.; Schroder, R. E. *Vac. Surf. Films* **1988**, 6, 14123.

(25) Sowers, A. T.; Ward, B. L.; English, S. L.; Nemanich, R. J. *J. Appl. Phys.* **1999**, 86, 3973.



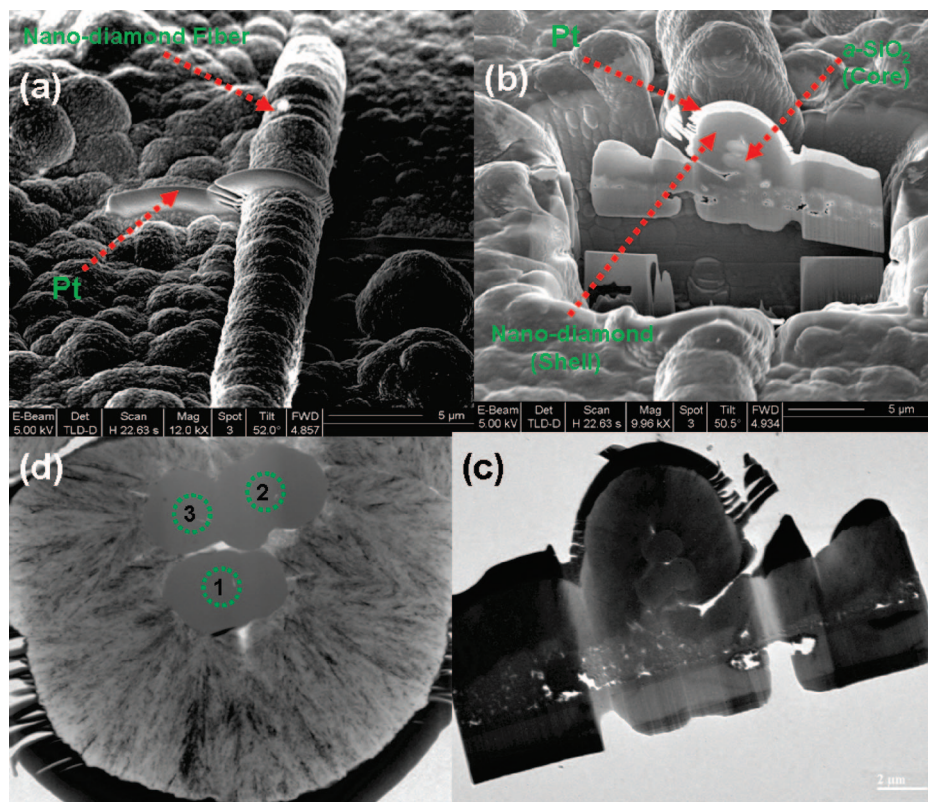


**Figure 5.** (a) FIB image in E-beam mode showing a NCD-coated  $\alpha$ -SiO<sub>2</sub> nanofiber lying on Si substrate and a protective layer of Pt  $\sim 2 \mu\text{m}$  thick coated on it. (b) FIB TEM image of specimen preparation in the final stage, ready for "lift-out". (c) Bright-field TEM image of specimen on copper TEM grid. (d) More magnified TEM image of specimen, from which we can easily observe a self-assembly of a cross-section of three  $\alpha$ -SiO<sub>2</sub> nanofibers (indicated by green dotted circles 1, 2, and 3, respectively). The  $\alpha$ -SiO<sub>2</sub> nanofibers (core) is conformally coated by nanometer-sized diamond grains (sheath).

carbon at the grain boundaries of NCD.<sup>26</sup> The analysis of micro-Raman studies confirms that the coated diamond is nanocrystalline in nature.

FIB TEM specimens were prepared by the lift-out method, which provides a rapid means of preparing an electron transparent cross-section from a specific site of interest. In this method, the diamond-coated sample was transferred inside the FIB chamber using a special sample holder, designed by FEI Company, for TEM sample preparation. FIB TEM specimen preparation follows various steps.<sup>18</sup> FIB image in E-beam mode (Figure 5a) shows a NCD-coated  $\alpha$ -SiO<sub>2</sub> nanofiber lying on the Si wafer and a protective layer of Pt  $\sim 2 \mu\text{m}$  previously deposited. Two trenches were milled on either side of the nanodiamond fiber (not shown) and the area in the middle was thinned by reducing the beam current to 300 pA. For high-resolution TEM photograph of the lattice and elemental analysis, the sample was thinned down to  $\sim 50$  nm. After polishing and thinning, the cross-section is cut free by the FIB (last step shown in Figure 5b). The specimen is then lifted-out with an electrostatic probe, which retrieves the free sample from its trench and deposits it on a TEM grid made up of copper.

A series of detailed morphological and structural investigations have also been carried out by HR-TEM and diffraction studies on the cross-section specimen of isolated nanodiamond fibers (as described above). Figure 5c shows a typical cross-sectional bright-field TEM image of the

specimen on a copper TEM grid. Figure 5d reveals more magnified TEM image of specimen, from which we can easily observe a cross-section of a self-assembly of three  $\alpha$ -SiO<sub>2</sub> nanofibers (indicated by green dotted circles 1, 2, and 3, respectively) residing as a core of the diamond fiber. The core region is conformally coated by nanometer-sized diamond grains (sheath). Figure 6a demonstrates the bright-field TEM image of interface region of  $\alpha$ -SiO<sub>2</sub> nanofibers (denoted by green dotted circle 1) and nanodiamond. For interfacial studies, electron diffraction was performed at various locations of the sheath and core regions, as indicated in Figure 6b.

The SAED obtained in the sheath region (red-dotted circle with green-dashed arrow 1) indicates the presence of the set of Debye's rings characteristics of the cubic diamond phase (space group  $Fd3m$ , cell parameter  $a_0 = 3.56 \text{ \AA}$ ). The experimental interplanar spacings (see Table 1) are found to match with the diamond reference values<sup>27</sup> with 1% uncertainty.

The intensity of the lattice planes in the SAED pattern decreases while scanning from the outer periphery toward the inner core region in the TEM image of the nanodiamond fiber specimen, revealing the change from crystalline to amorphous phase. The diffraction pattern was taken from three different regions, sheath, interface and core (Figure 6b, red-dotted circles 1, 2, and 3, respectively). The low intensity of the planes indicates the amorphous nature at the interface.

(26) Ferrari, A. C.; Robertson, J. *Phys. Rev. B* **2000**, *61*, 14095.

(27) Joint Committee for Powder Diffraction Standards-International Centre for Diffraction Database (JCPDS-ICDD) PDF 06-0675; CDF 037638.

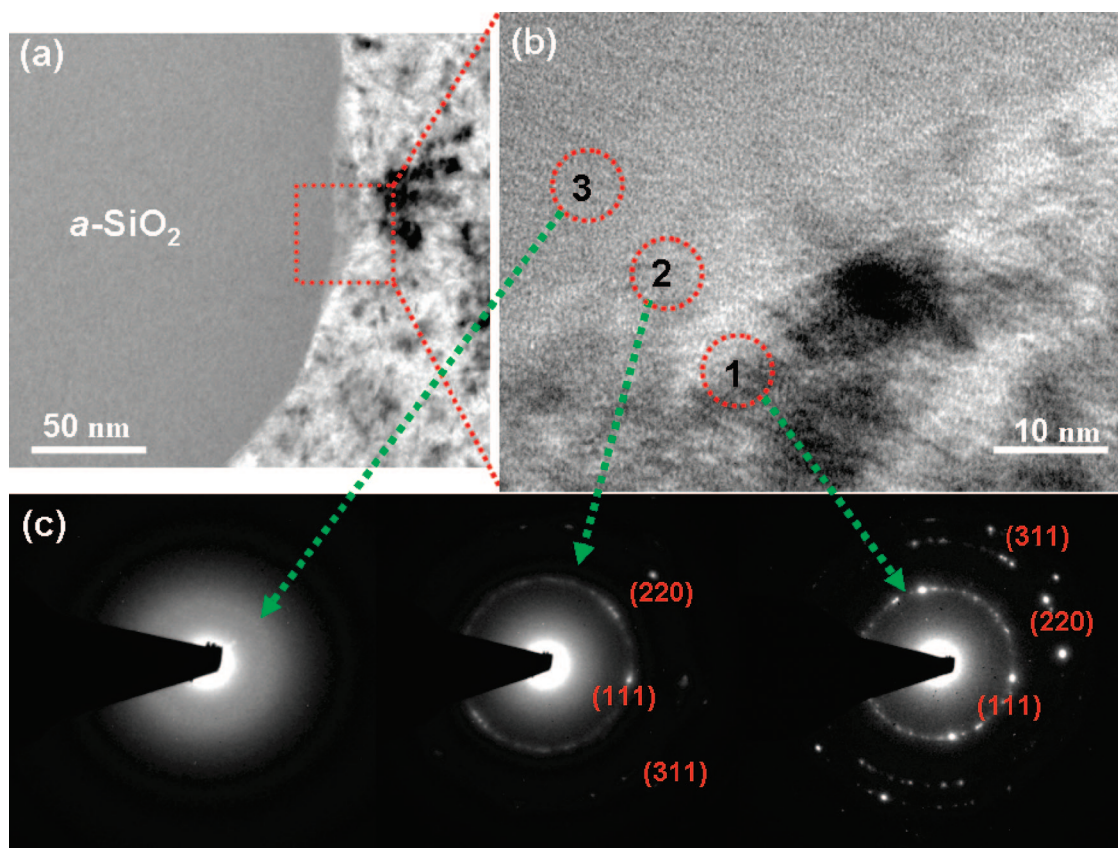


**Figure 6.** (a) Typical cross-section bright-field TEM image of a NCD fiber specimen where the core ( $a\text{-SiO}_2$ ) and sheath (diamond) regions are clearly observed. (b) Magnified image of the red-dotted square region marked in (a). (c) SAED patterns collected from sheath, interface and core regions (right to left), corresponding to green-dashed arrows with red-dotted circles 1, 2, and 3, respectively.

**Table 1. Spacing ( $d$ ) and Indexing ( $d_{hkl}$ ) of Electron-Diffraction Patterns (see Figure 6c) Collected from Sheath, Interface, And Core Regions Identified in Figure 6b**

selected regions	$d$ -spacing		$d_{hkl}$
	experimental $d$ (Å)	theoretical <sup>22</sup> diamond $Fd3m$ , $a_0 = 3.56$ Å $d$ (Å)	
spot 1 (sheath)	2.06	2.0592	111
	1.27	1.2610	220
	1.07	1.0754	311
spot 2 (interface)	2.05	2.0592	111
	1.26	1.2610	220
	1.08	1.0754	311
spot 3 (core)			

The combination of EDS and PEELS with high-angle annular dark-field (HAADF) imaging technique can provide detailed information on the composition, chemistry and structure (electronic and crystal) of nanoscale systems with atomic resolution and sensitivity.<sup>28</sup> Figure 7a shows HAADF image of core–sheath region of FIB TEM specimen in which there are three microfibers integrated with each other in self-organization mechanism. Elemental profiles across a core-sheath region (see Figure 7a, indicated by red line 1) were obtained by scanning a finely focused electron probe size of  $\sim 0.5$  nm. The K-edge weights were normalized for chemical profiling of all of the elements except for Si for which the L-edge was used; therefore, the profiles represent the distribution of atomic concentrations.<sup>29,30</sup> Figure 7b reveals the profiles of Si, O and C elements present in the NCD

fiber. Figure 7c shows Si and O profiles, in which Si:O ratio is very near 1:2, which indicates that the core region is  $a\text{-SiO}_2$ . The inner diameter of C profile (see Figure 7d) is close to the outer diameter of the Si and O profiles. Figure 7e shows EDS measurement at the core region (indicated by a red plus sign in Figure 7a) which further confirms that in this experiment the as-grown  $a\text{-SiO}_2$  nanofibers were used as a templates for the synthesis of high-density NCD fibers.

We have also performed HR-TEM and PEELS measurements near the interface of core-sheath region, to study the growth mechanism in detail. Figure 8a shows the HR-TEM image performed at the interface (indicated by the blue-dashed line) of the core-sheath region, where we can distinguish amorphous and crystalline regions. The interface is clearly visible. The inset shows diffuse rings collected from a thin layer of  $a\text{-C}$  near the core surface region (between the  $a\text{-SiO}_2$  and the nanocrystalline diamond). This indicates that nanodiamond (grain size  $\sim 15$  nm) does not nucleate directly on the  $a\text{-SiO}_2$  surface. Instead, an intermediate layer of  $a\text{-C}$  is formed, and the nanodiamond nucleates directly on the  $a\text{-C}$  during CVD growth. The HR-TEM images (Figure 8a,b) reveal an interlayer spacing of about  $2.10 \pm 0.05$  Å, which is consistent with the expected spacing from (111) diamond planes of 2.06 Å. A highly magnified view of diamond lattice planes marked by the white dotted square

(28) Liu, J. J. *Electron Microsc.* **2005**, *54*, 251.

(29) Colliex, C. J. *Electron Microsc.* **1996**, *45*, 44.

(30) Egerton, R. F. *Electron Energy-Loss Spectroscopy in the Electron Microscope*, 2nd ed.; Plenum: New York, 1996)



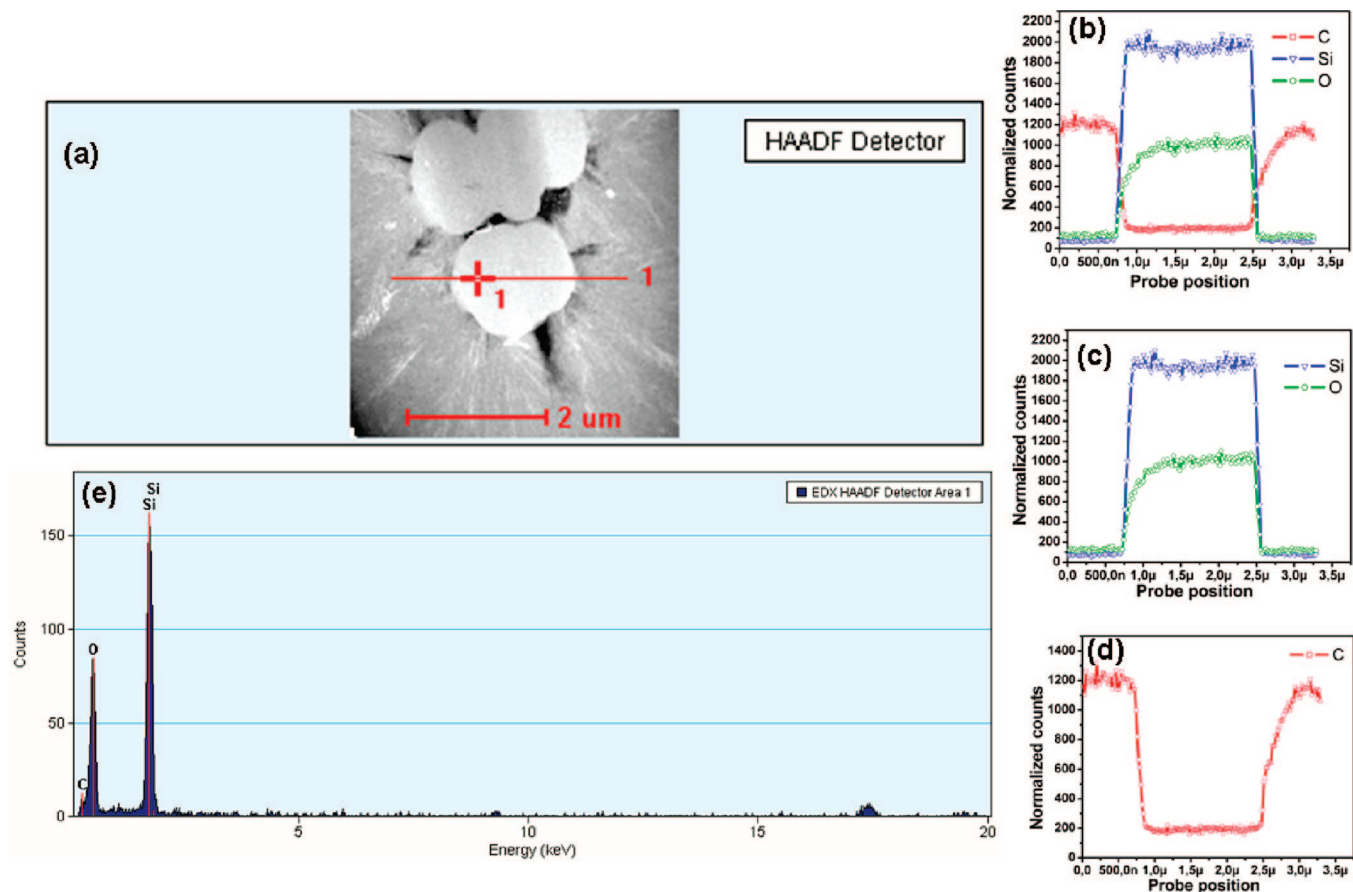


**Figure 7.** (a) High-angle annular dark-field (HAADF) image of core-sheath region of FIB TEM specimen which clearly shows three fibers were integrated with each other in self-organization mechanism. (b) Profiles of all the elements present in the core-sheath region (indicated by red line 1) (c) Si and O profiles, in which the Si:O ratio is very near 1:2, which indicates that the core region is  $\alpha$ -SiO<sub>2</sub>. (d) Inner diameter of C profile close to the outer diameter of the Si and O profiles. (e) EDS measurement performed at the core region (indicated by red plus sign in a).

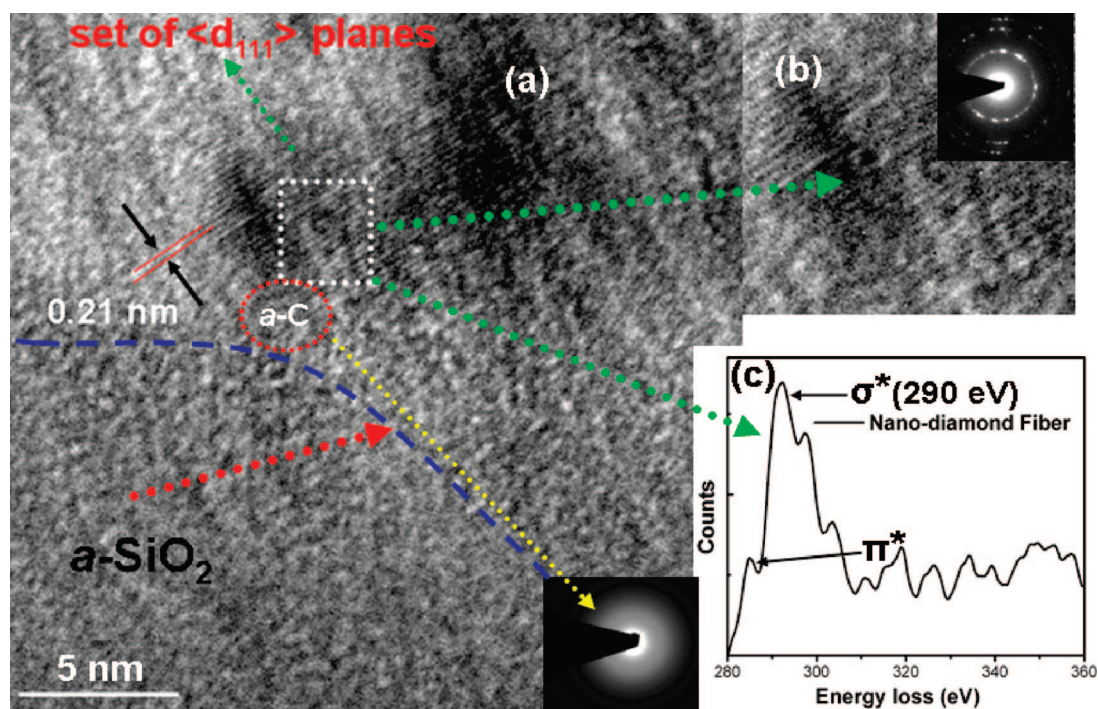


**Figure 8.** (a) HR-TEM images taken at the interface (indicated by blue-dashed line) of the core-sheath region, discriminating the  $\alpha$ -SiO<sub>2</sub> surface and the nanodiamond grain. Lower inset: diffuse rings collected from a thin layer of a-C near the core surface region. (b) Highly magnified view of a set of  $\langle 111 \rangle$  diamond lattice planes. Inset: corresponding SAED pattern. (c) Carbon K-edge loss spectra taken from NCD grain.

in Figure 8a is shown in Figure 8b. The inset shows crystalline rings in the SAED pattern taken from diamond lattice planes.

The PEELS in TEM has proved to be a powerful technique for studying the electronic structure of materials.<sup>31</sup> Recently, Brusill et al.<sup>32</sup> carefully performed the structural analysis of nanocrystalline diamond powder by using HR-TEM/PEELS. In our present work, PEELS spectra were acquired in the imaging mode using 3 mm PEELS entrance aperture with a probe size of  $\sim 0.2$ – $0.5$  nm and a measured current of  $\sim 0.15$  nA. Figure 8c shows the PEELS spectra taken from the area indicated by the white-dotted square in Figure 8a. We can see the carbon K-edge (that is, excitations from the carbon  $1s$  orbital to states above the Fermi level) loss spectra taken from nanocrystalline diamond grain. It exhibits a peak at 290 eV due to  $\sigma^*$  states. A very low intensity peak appears at  $\sim 285$  eV, corresponding to  $\pi^*$  states. The PEELS above 290 eV is similar to that of diamond<sup>33</sup> and is different from that of graphite or  $sp^3$ -rich tetrahedral amorphous carbon.<sup>34</sup> Gruen et al.<sup>35</sup> suggested that the weak peak at 285 eV is due to  $\pi$ -bonded carbons which are present at the grain boundaries of nanocrystalline diamond. It was also demonstrated from the theoretical point of view<sup>36</sup> that  $sp^2$  bondings are energetically stable in grain boundaries of nanocrystalline diamond.

## Conclusion

High-density NCD fibers with lengths of 50–100  $\mu\text{m}$  and diameters of 1–5  $\mu\text{m}$  were prepared for the first time using  $\alpha$ - $\text{SiO}_2$  nanofiber template. The templates were synthesized by conventional VLS method followed by conformal coating of as-synthesized templates with 15–20 nm-sized NCD grains using MPECVD technique in hydrogen-deficient condition. The growth mechanism and phases formation of NCD-coated  $\alpha$ - $\text{SiO}_2$  nanofiber is clearly explained. The nanocrystalline nature of the diamond material is confirmed by micro-Raman and PEELS studies. Perfect crystallinity of the sample is further confirmed from SAED patterns. The HR-TEM studies (at the interface of core and sheath regions) reveal an interlayer spacing of about  $2.10 \pm 0.05$  Å, which is in agreement with the expected spacing from (111) diamond planes of 2.06 Å. Unlike other reports on NCD fibers,<sup>37,38</sup> the present method can produce isolated nanocrystalline diamond fibers at high growth rates. This novel material is expected to find applications in cold-cathode devices,<sup>39</sup> heat sinks in microelectronics and structural materials in micro- and nanoelectromechanical systems.<sup>40</sup>

CM0714741

- 
- (31) Kimoto, K.; Sekiguchi, T.; Aoyama, T. *J. Electron Microsc.* **1997**, *46*, 369.
  - (32) Peng, J. L.; Fehlhaber, R. P.; Bursill, L. A.; McCulloch, D. G. *J. Appl. Phys.* **2001**, *89*, 6204.
  - (33) Egerton, R. F.; Whelan, M. J. *J. Electron Spectrosc. Relat. Phenom.* **1974**, *3*, 232.
  - (34) Bruley, J.; Williams, D. B.; Cuomo, J. J.; Pappas, D. P. *J. Microscopy* **1995**, *180*, 22.

- 
- (35) Gruen, D. M. *Annu. Rev. Mater. Sci.* **1999**, *29*, 211.
  - (36) Koblinski, P.; Wolf, D.; Phillpot, S. R.; Gleiter, H. *J. Mater. Res.* **1998**, *13*, 2077.
  - (37) Terranova, M. L.; Orlanducci, S.; Fiori, A.; Tamburri, E.; Sessa, V. *Chem. Mater.* **2005**, *17*, 3214.
  - (38) Rossi, M.; Terranova, M. L.; Piccirillo, S.; Sessa, V.; Manno, D. *Chem. Phys. Lett.* **2005**, *402*, 340.
  - (39) Zhu, W.; Kochanski, G.; Jin, S.; Seibles, L. *J. Appl. Phys.* **1995**, *78*, 2707.
  - (40) Espinosa, H. D.; Peng, B.; Prorok, B. C.; Auciello, O.; Carlisle, J. A.; Gruen, D. M.; Mancini, D. C. *J. Appl. Phys.* **2003**, *94*, 6076.